Lensing effects on the CMB

MATIAS ZALDARRIAGA

NYU & IAS

LENSING

LARGE SCALE STRUCTURE + ANISOTROPIES

The power spectrum of the projected mass density can be written in terms of the PS of the 3D mass fluctuations.

$$C_\ell^{\kappa\kappa} = 18\pi^3 \Omega_m^2 H_0^4 \int_0^{\chi_0} d\chi \frac{g^2(\chi,\chi_0)}{a^2(\chi)\, r^2(\chi)} P_\delta\left(k=\frac{\ell}{r(\chi)},\chi\right)$$

$$g(\chi',\chi) = \frac{r(\chi')\, r(\chi-\chi')}{r(\chi)}$$

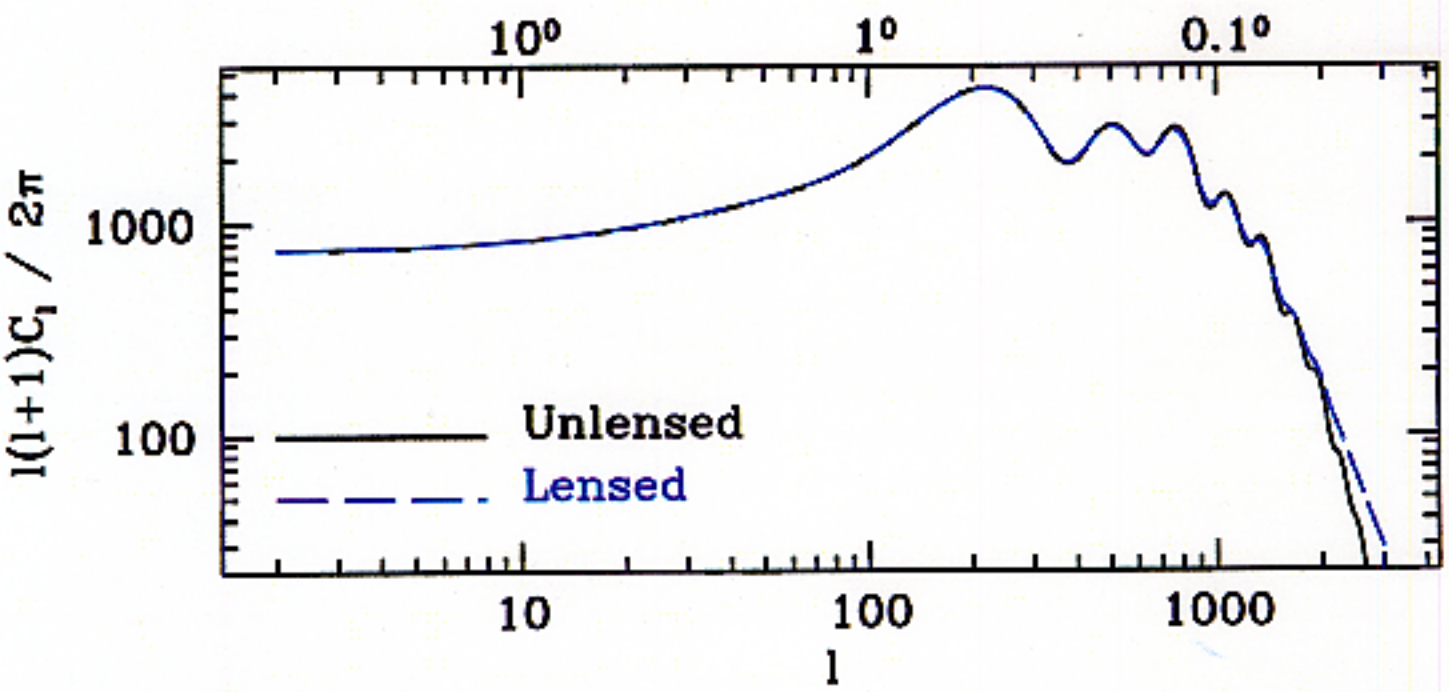
10°
1°
0.1°
1000
100
l(l+1)C_l / 2π
Unlensed
Lensed
10
100
1000
l

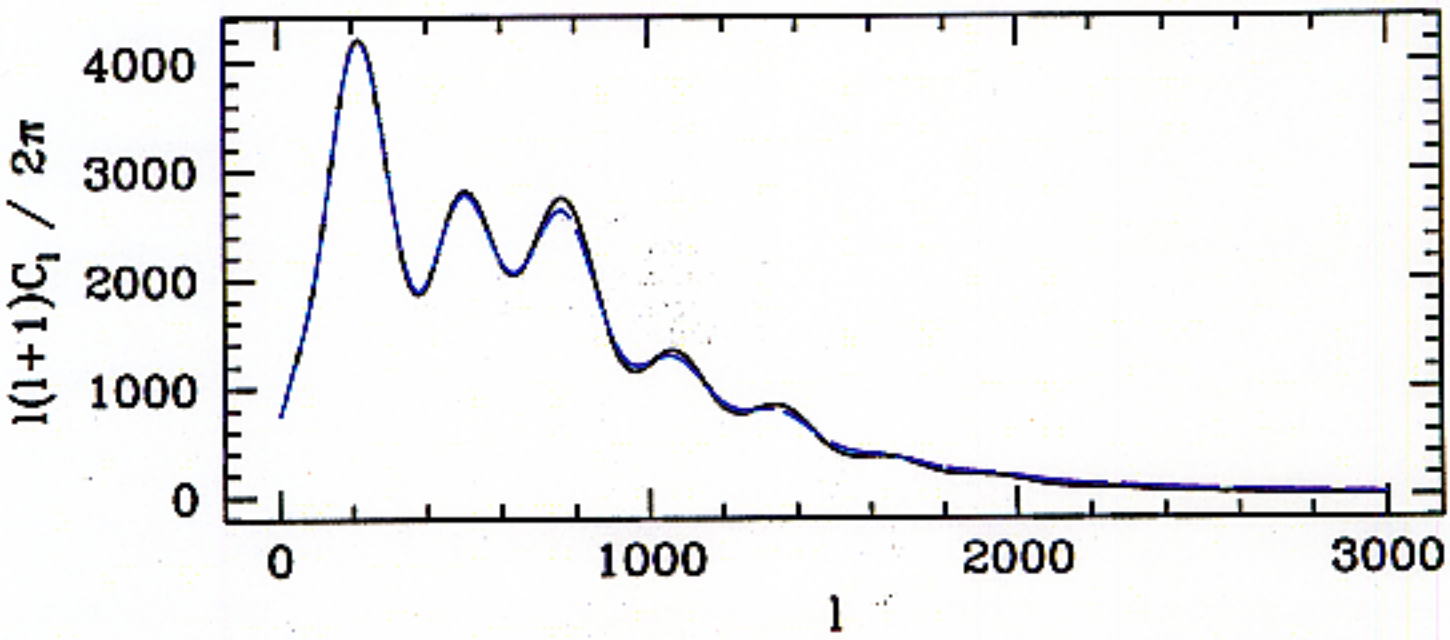
4000
3000
2000
1000
0
l(l+1)C_l / 2π
0
1000
2000
3000
l

E-B Decomposition

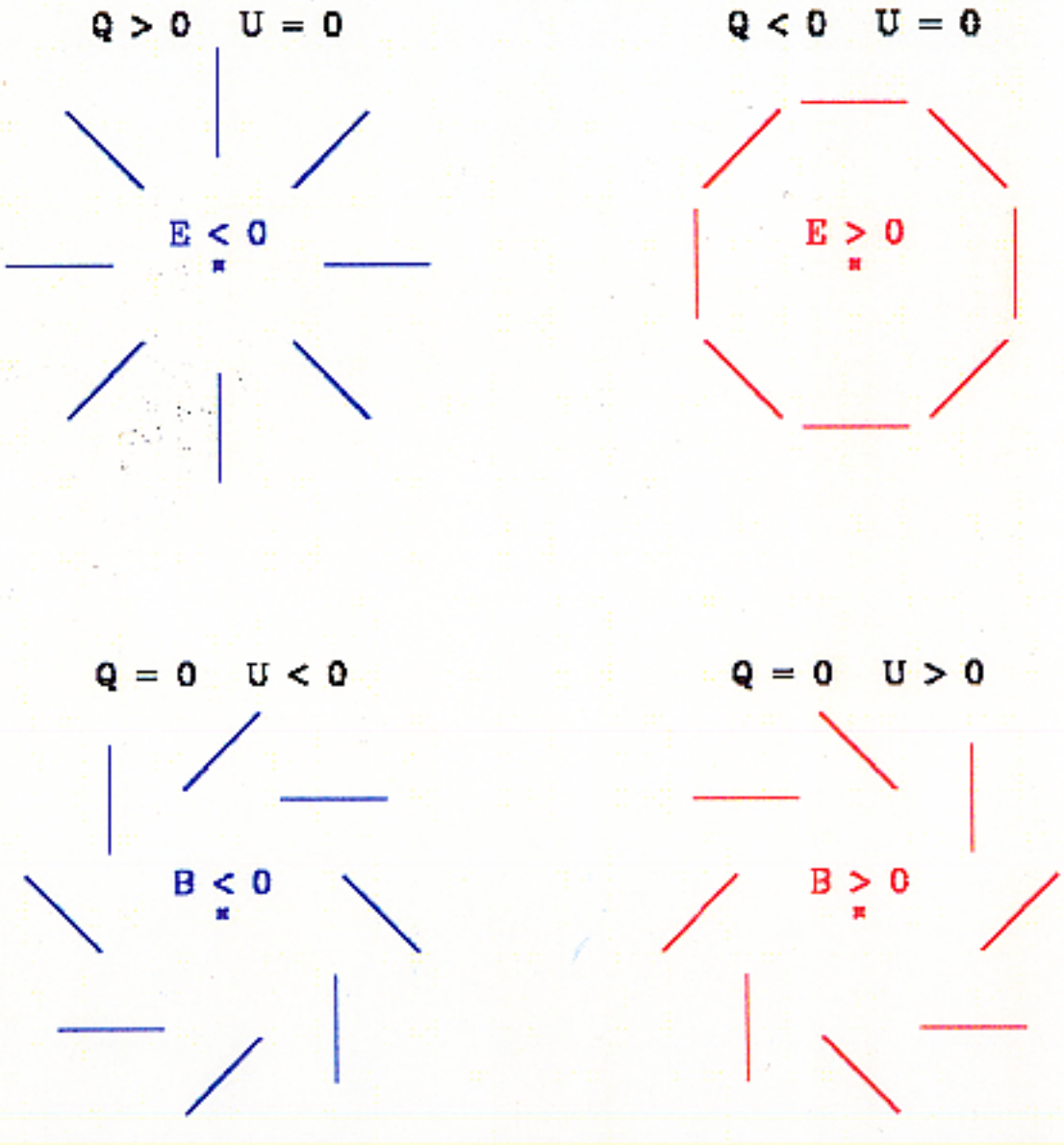

Seljak & MZ
Kamionkowski
Kosowsky &
Stebbins

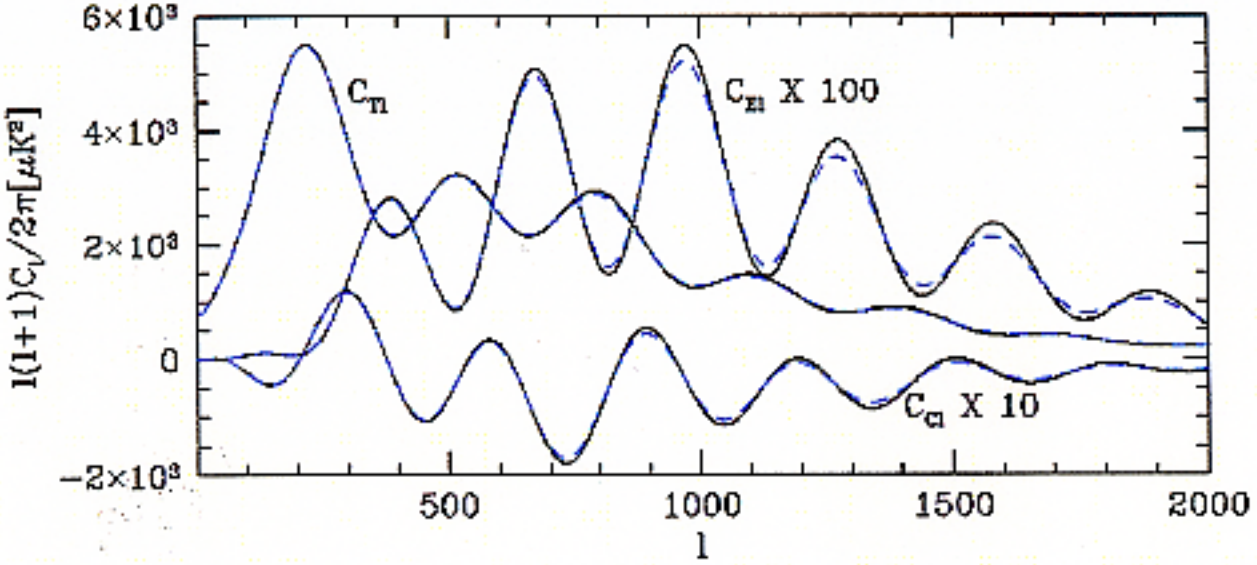

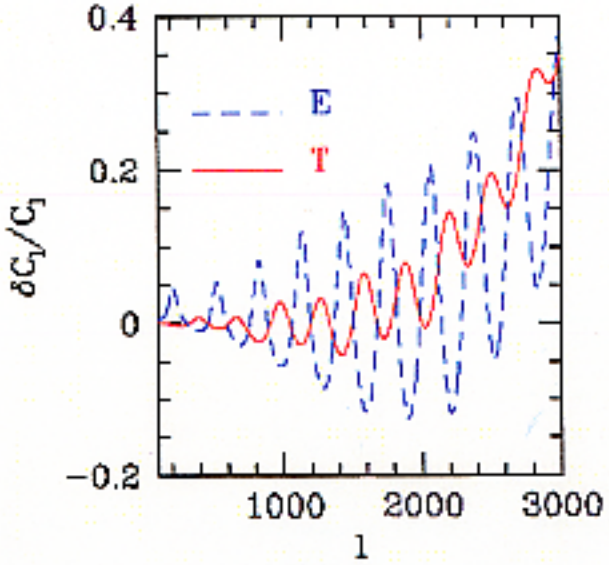

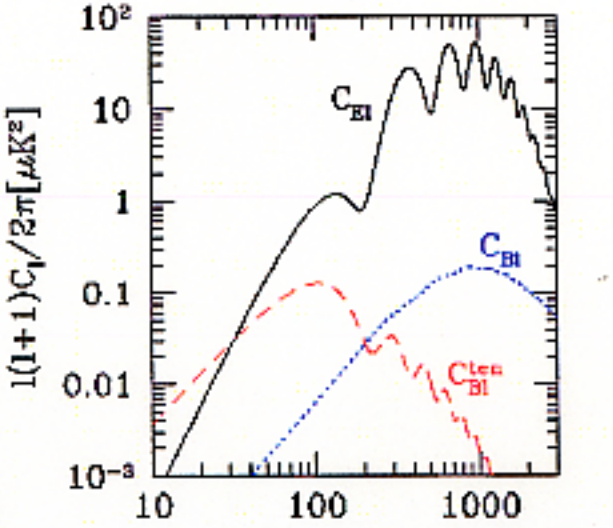

Zaldarriaga & Seljak
1996

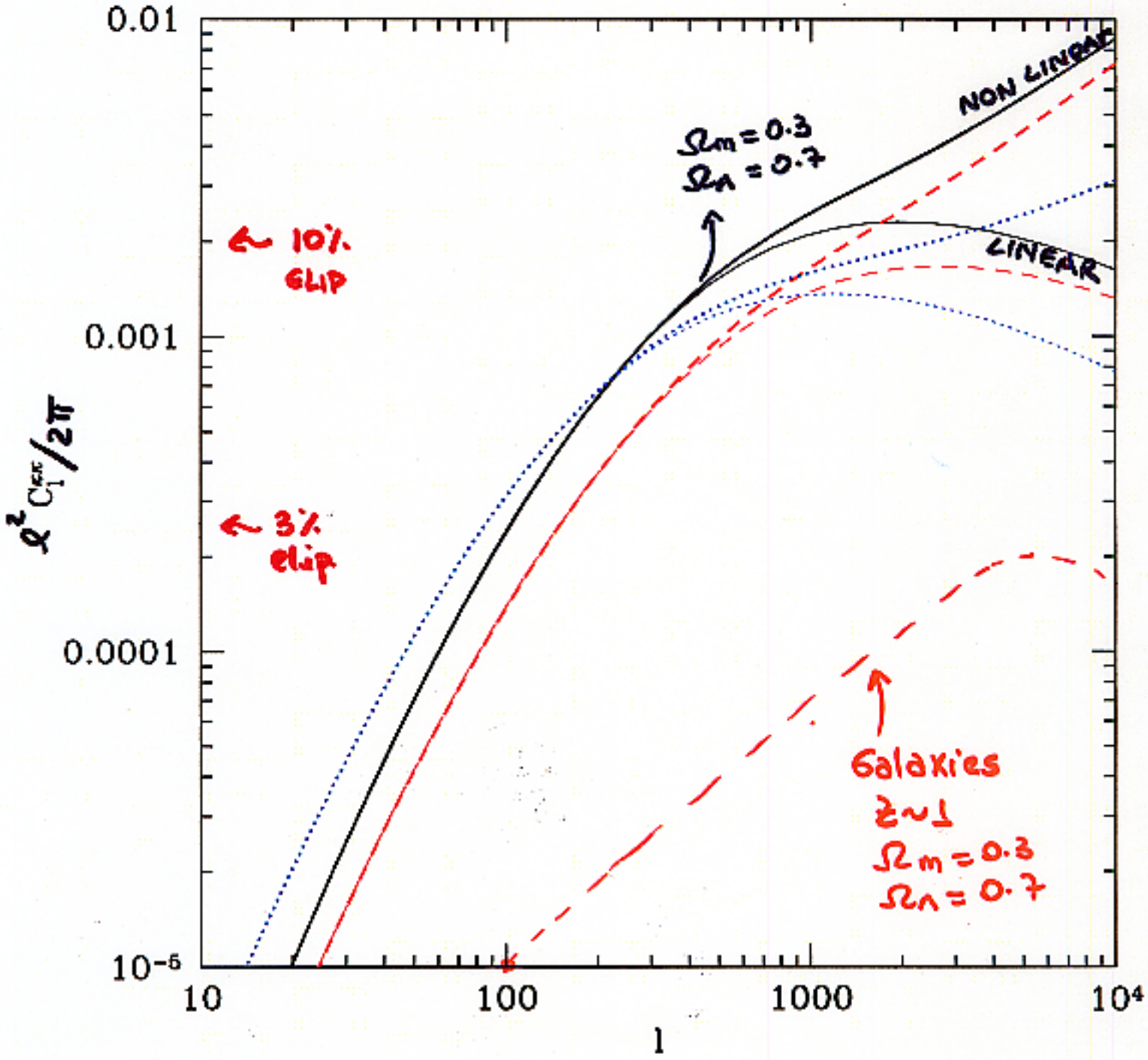
0.01
0.001
0.0001
10^{-5}
10
100
1000
10^4
l
$l^2 C_l^{\kappa\kappa}/2\pi$
NON LINEAR
LINEAR
$\Omega_m = 0.3$
$\Omega_\Lambda = 0.7$
← 10% slip
← 3% slip
Galaxies
$z \sim 1$
$\Omega_m = 0.3$
$\Omega_\Lambda = 0.7$

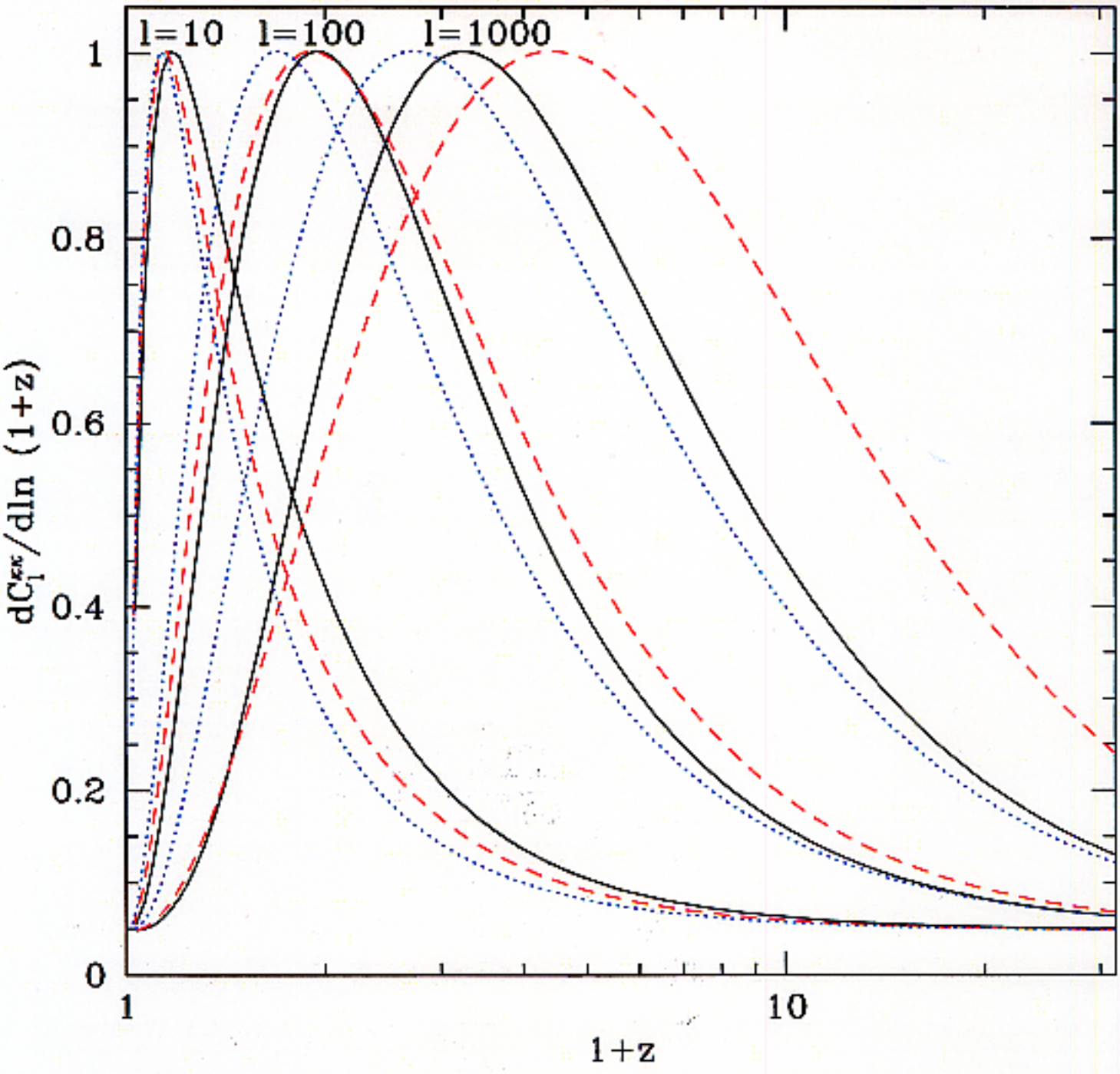
l=10
l=100
l=1000
1
0.8
0.6
0.4
0.2
0
$dC_l^{\kappa\kappa}/d\ln(1+z)$
1
10
1+z

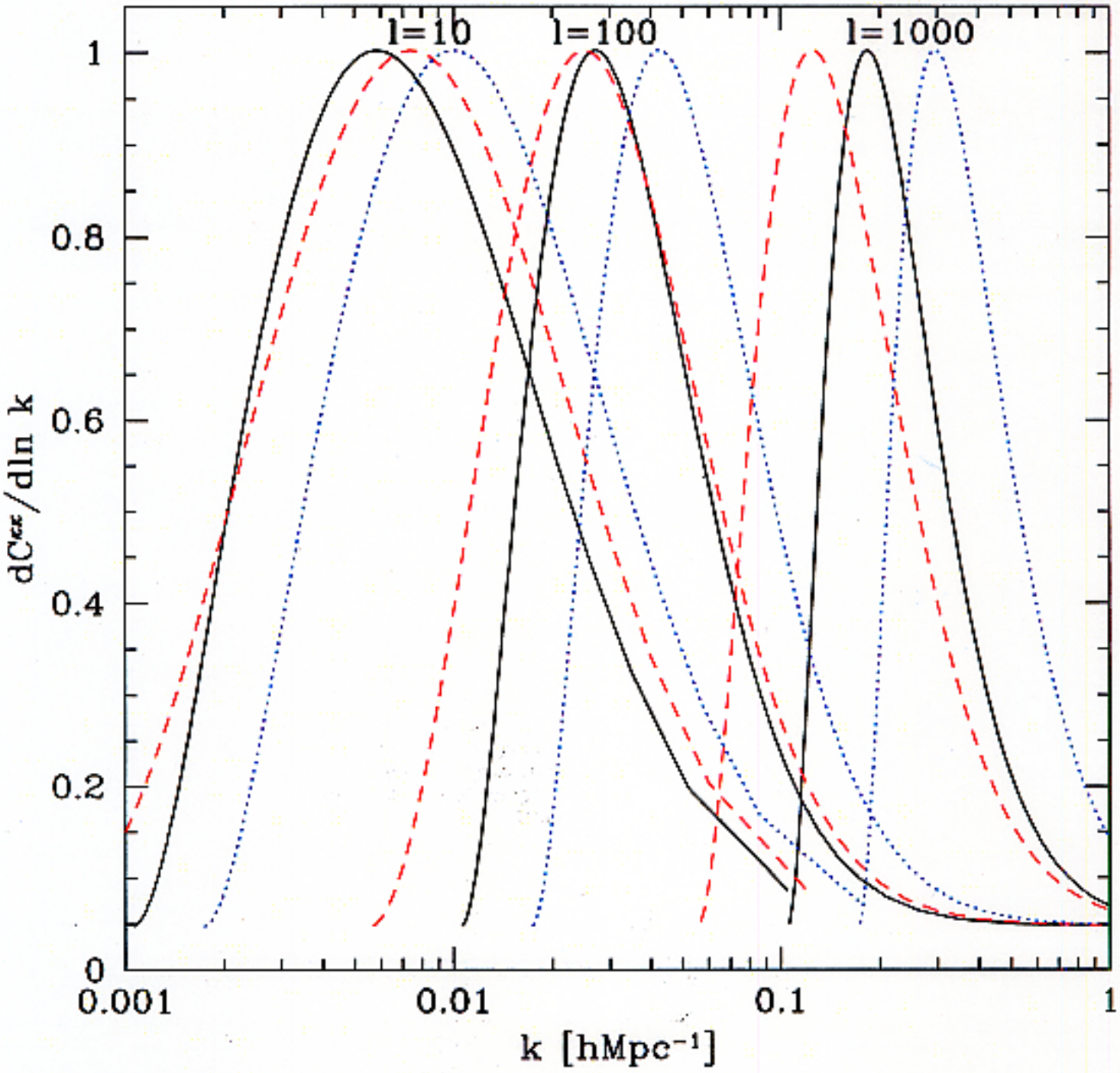

$$\lambda = \frac{2\pi}{k} \approx 600 \left(\frac{0.01\ h\mathrm{Mpc}^{-1}}{k}\right) \mathrm{Mpc}$$

Inferred matter fluctuations at present epoch

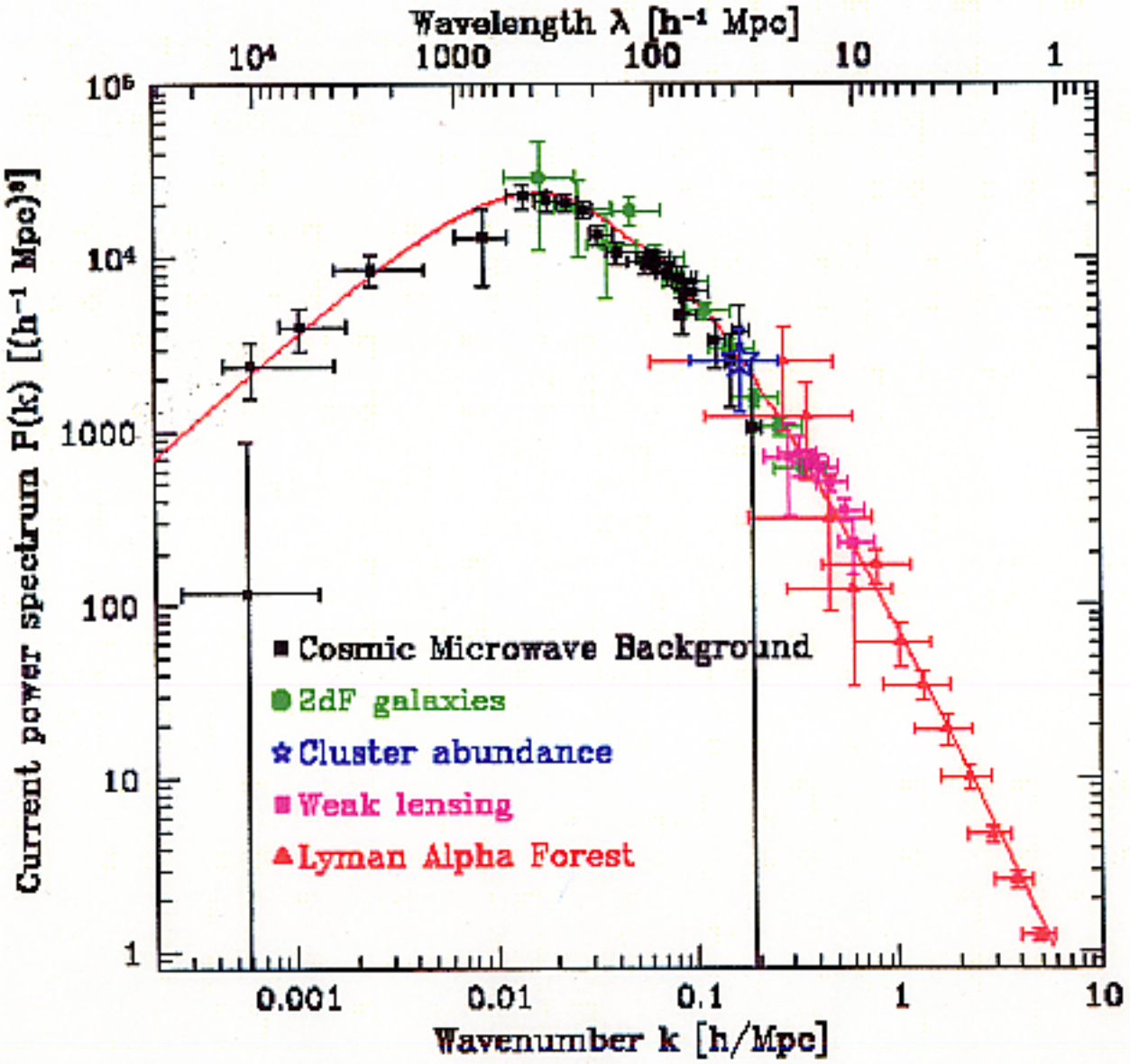

Tegmark & MZ

Large scale matter fluctuations distorting

small scale temperature anisotropies

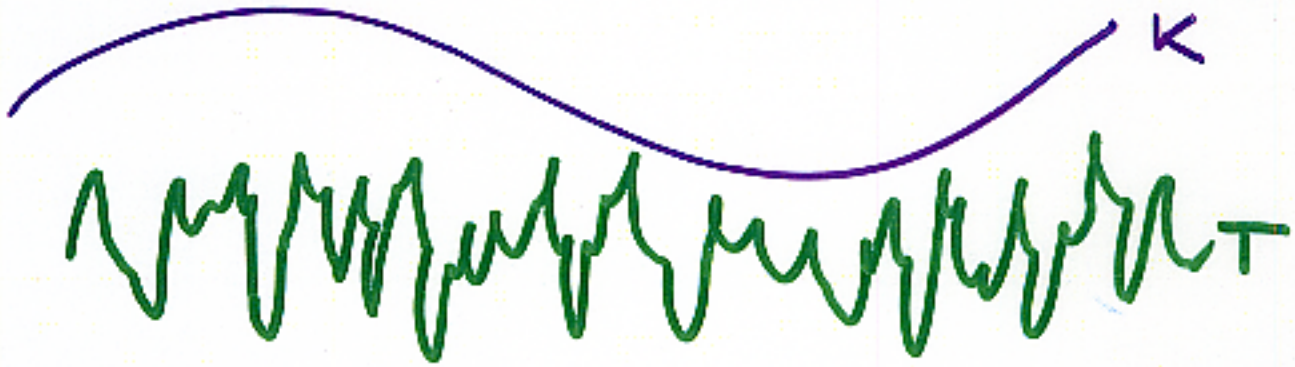

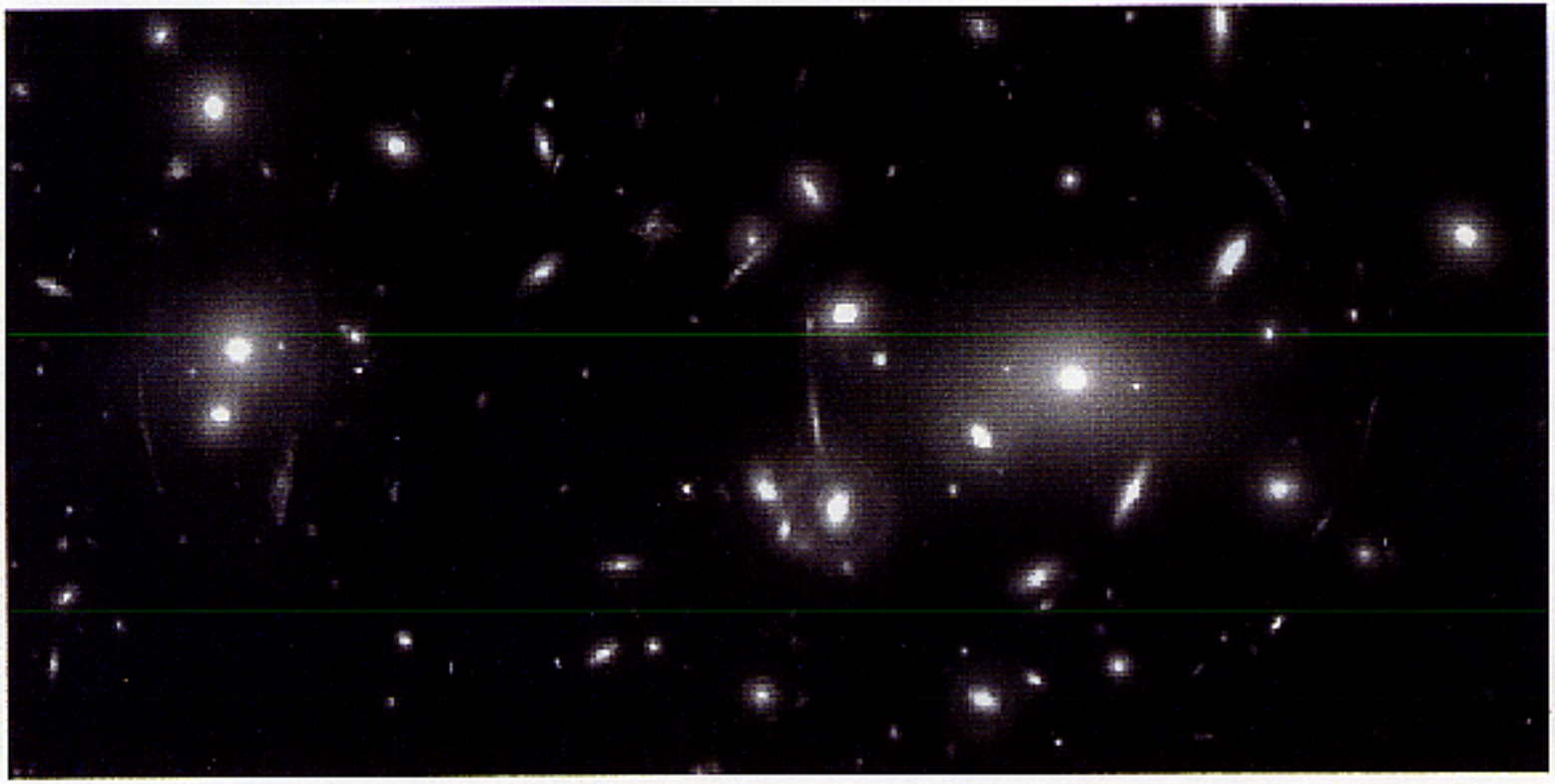

A2218

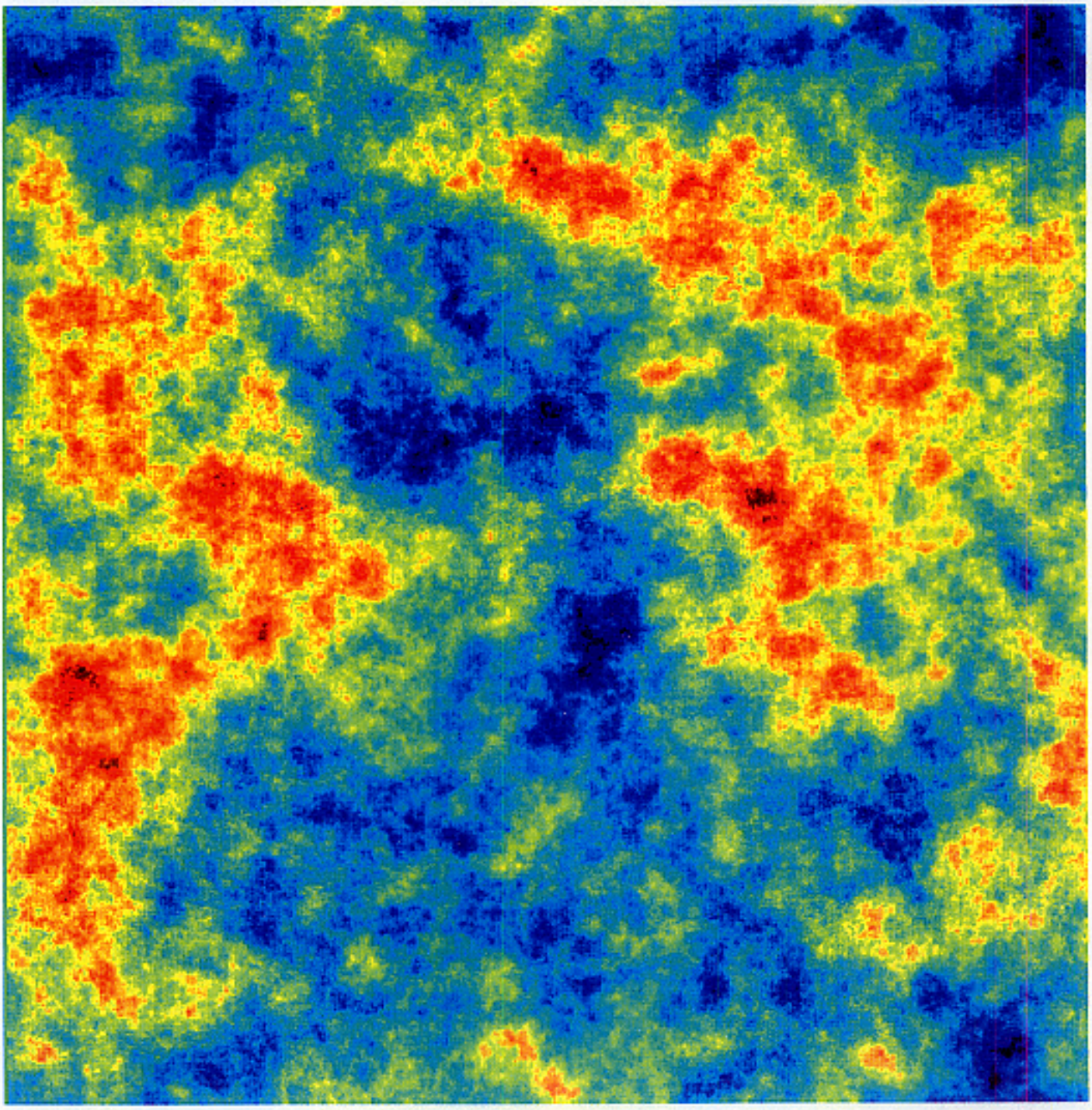

6'x6'

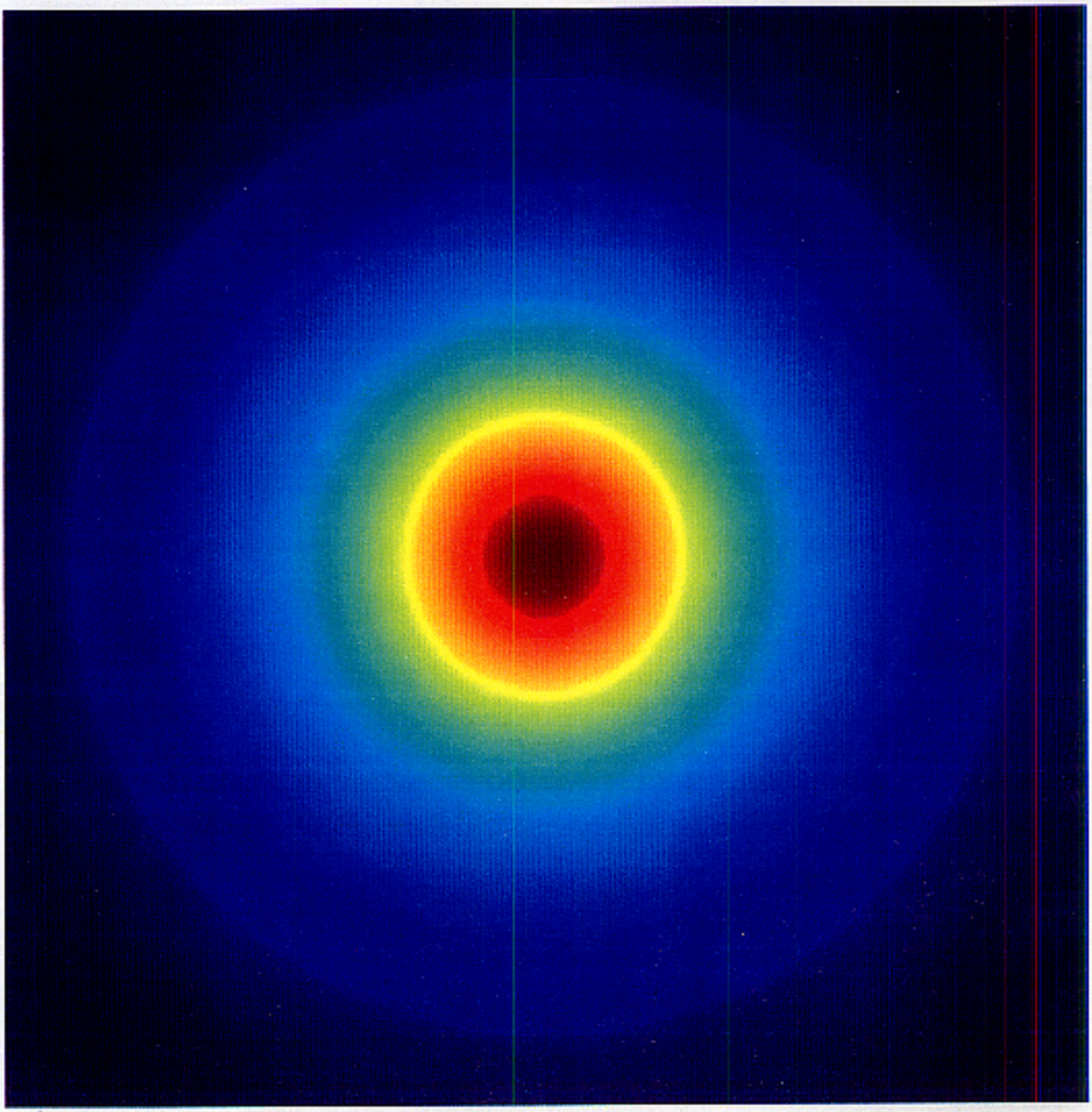

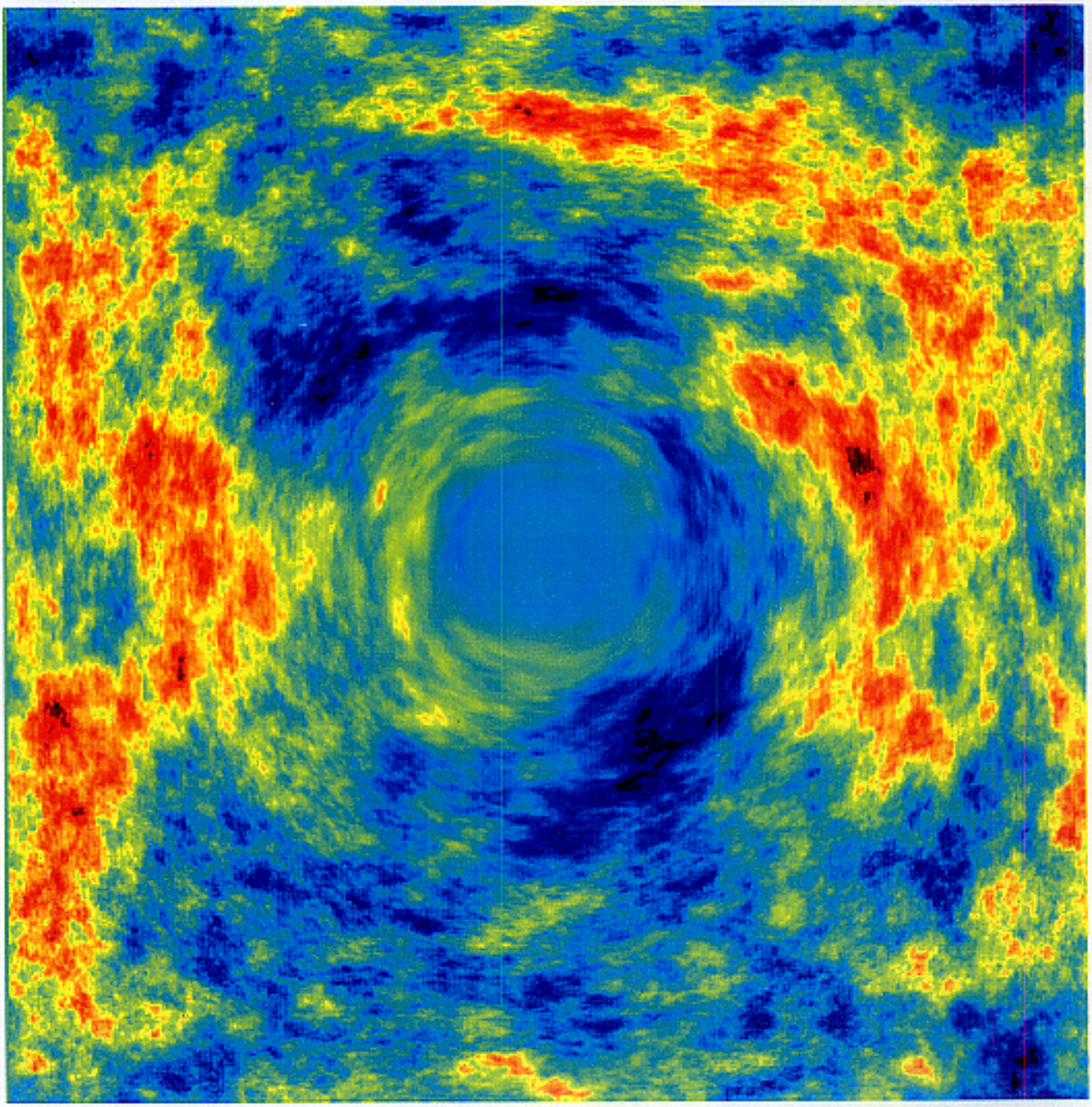

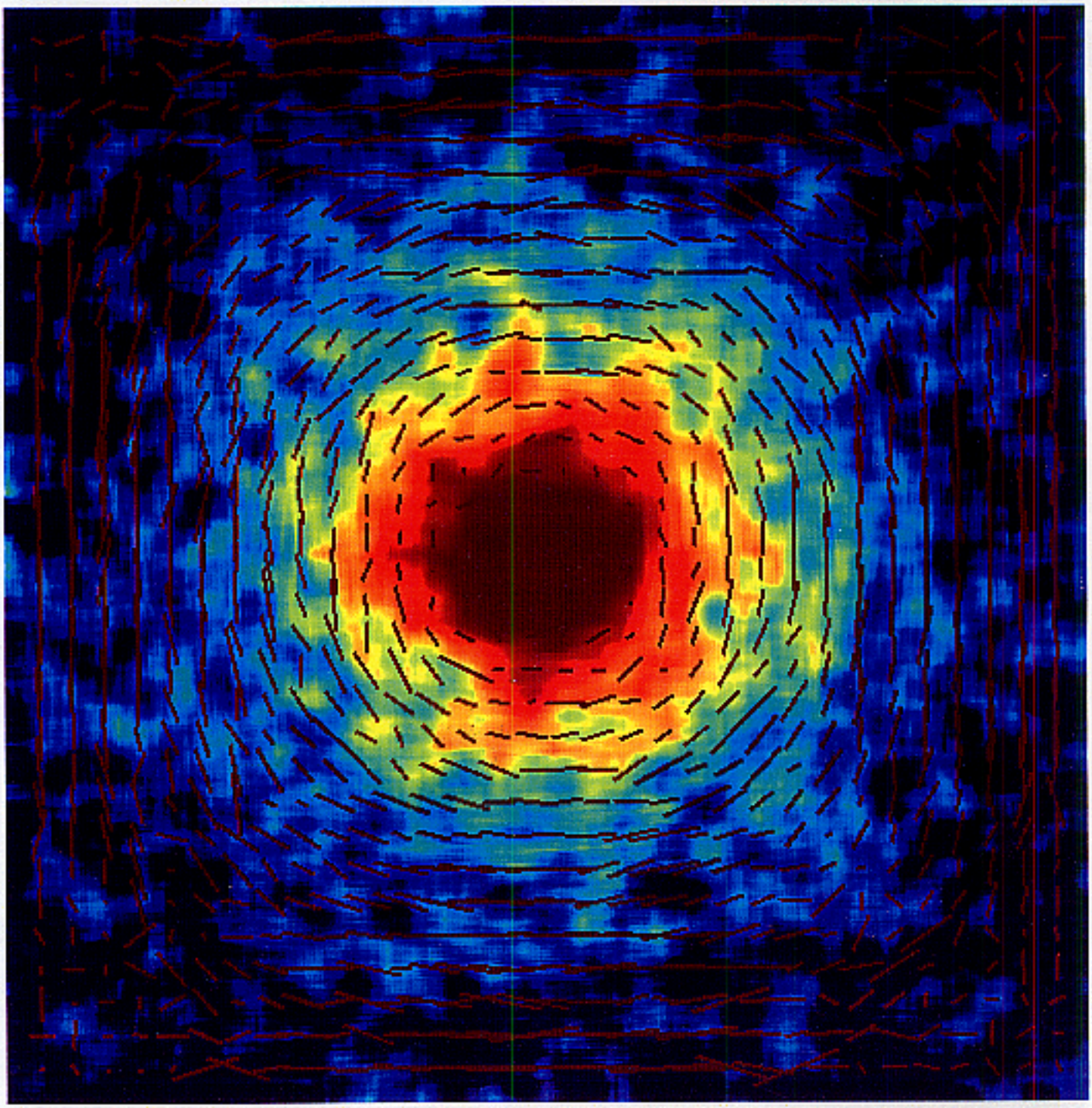

Method

$$\tilde{Q} \equiv (T_x^2 - T_y^2)(\vec{\theta})$$

$$\tilde{U} \equiv (2 T_x T_y)(\vec{\theta})$$

$$\tilde{S} \equiv (T_x^2 + T_y^2)(\vec{\theta})$$

$$\langle \tilde{Q} \rangle_{CMB} = -2\gamma_1 \sigma_S^2$$

$$\langle \tilde{U} \rangle_{CMB} = -2\gamma_2 \sigma_S^2$$

$$\langle \tilde{S} \rangle_{CMB} = (1-2\kappa)\sigma_S^2$$

UNLENSED T

$$\sigma_S^2 = \langle \tilde{T}_x^2 + \tilde{T}_y^2 \rangle_{CMB}$$

$$\kappa(\vec{e}) = \gamma_1(\vec{e}) \cos 2\phi_e + \gamma_2(\vec{e}) \sin 2\phi_e$$

$$0 = -\gamma_1(\vec{e}) \sin 2\phi_e + \gamma_2(\vec{e}) \cos 2\phi_e$$

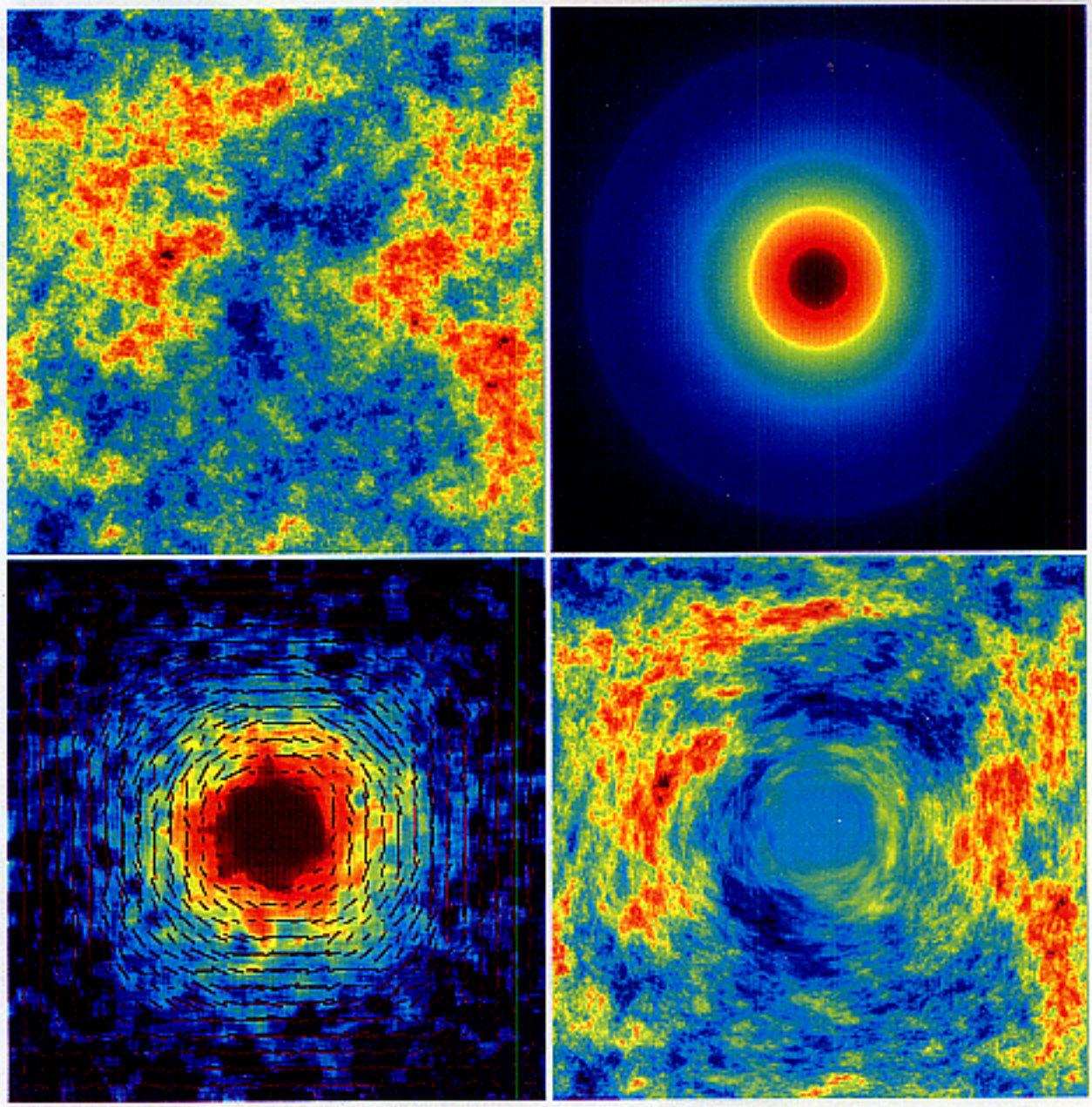

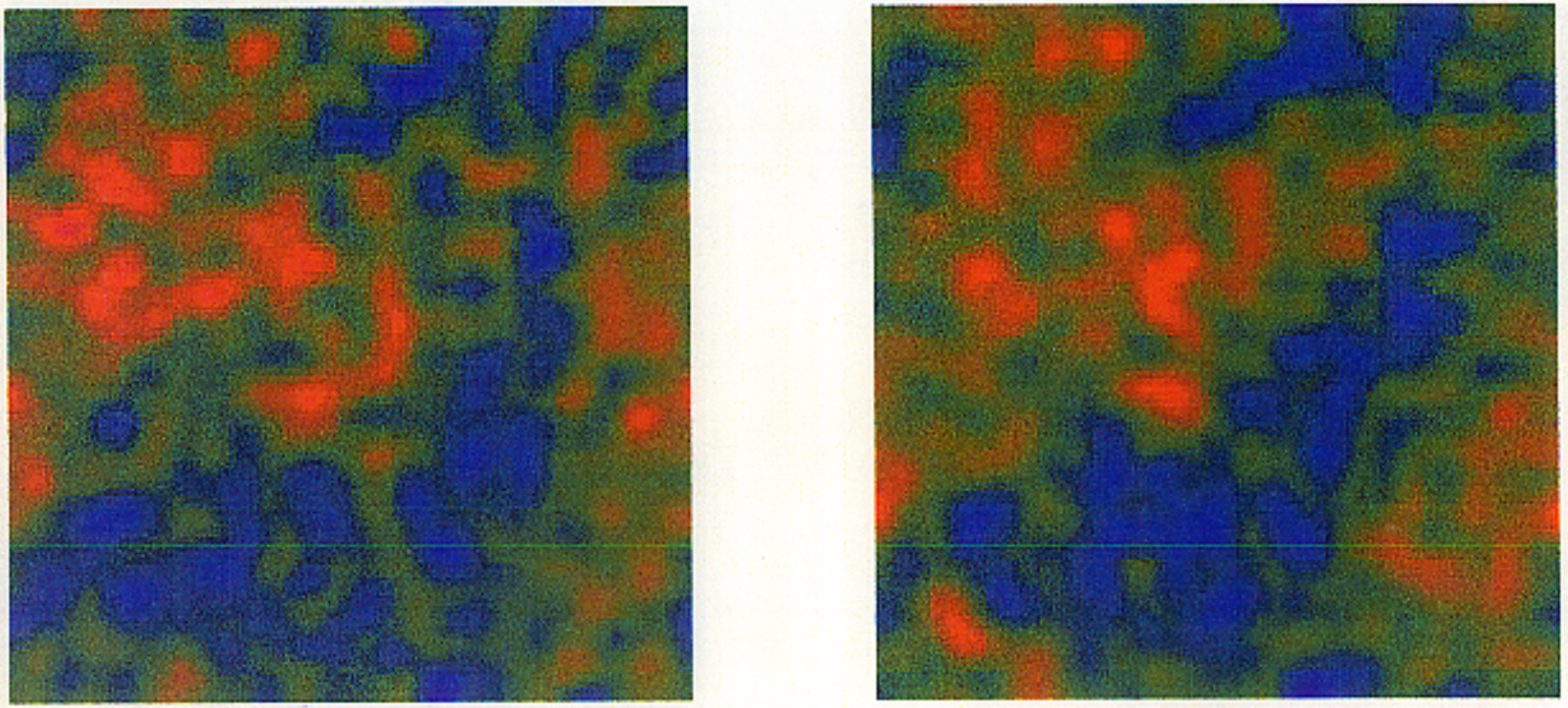

FIG. 3.— Top: A $32^\circ \times 32^\circ$ realization of the deflection field in the ΛCDM model. Bottom: Recovery of the deflection field with a $\sigma = 1.5'$ beam (FWHM) and detector noise of $w^{-1/2} = 10$ (10^{-6}-arcmin).

W. Hu
astro-ph/0105424

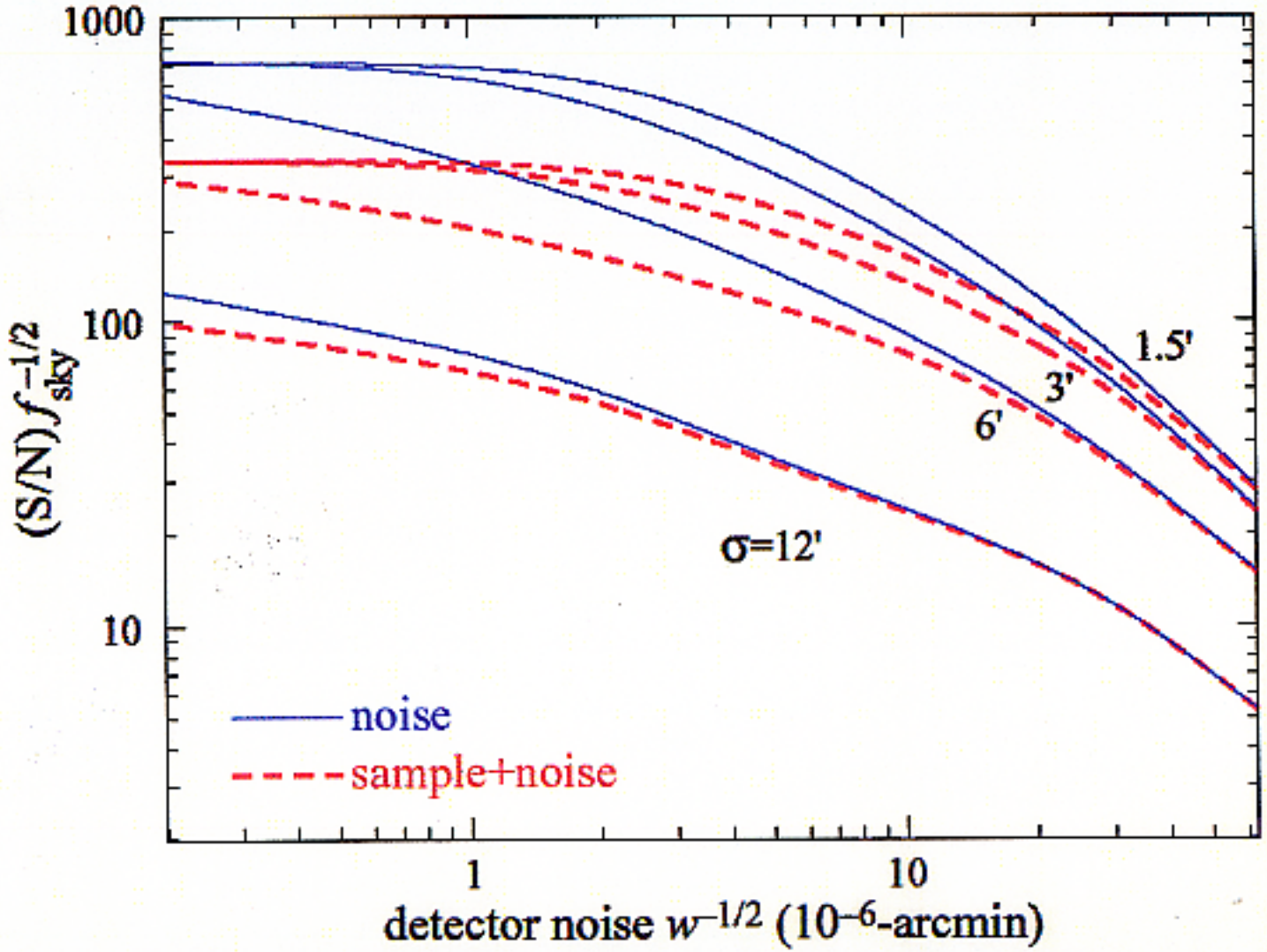

FIG. 4.— Signal-to-noise as a function of detector noise, beam and sky fraction $f_{\rm sky}$. Solid lines include both sample and Gaussian noise (primary CMB and instrumental) variance; dashed lines include only Gaussian noise variance. The signal-to-noise drops off rapidly for $w^{-1/2} > 15$ (10^{-6}-arcmin) and FWHM beams $\sigma > 5'$.

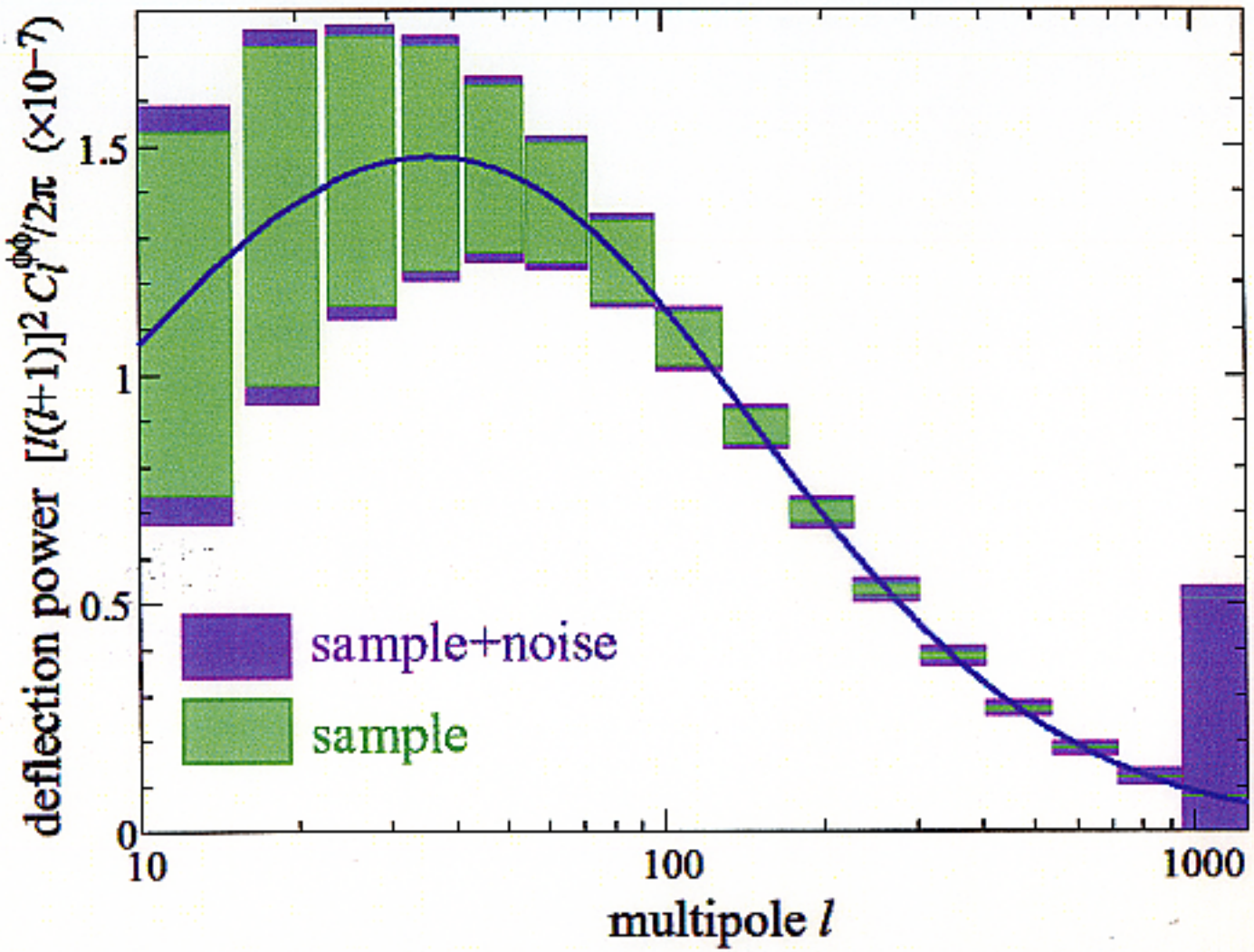

FIG. 1.— Lensing deflection power spectrum for the ΛCDM model. Error bars represent the total (sample plus noise) variance and sample variance from recovery from an area of $f_{\rm sky} = 0.1$ and an experiment with a beam of $\sigma = 1.5'$ and noise $w^{-1/2} = 10$ (10^{-6}-arcmin). Note that the errors for $L \lesssim 200$ are dominated by sample variance implying that the recovered map has high signal-to-noise.

W. Hu
astro-ph/0105424

Cleaning the B-Modes

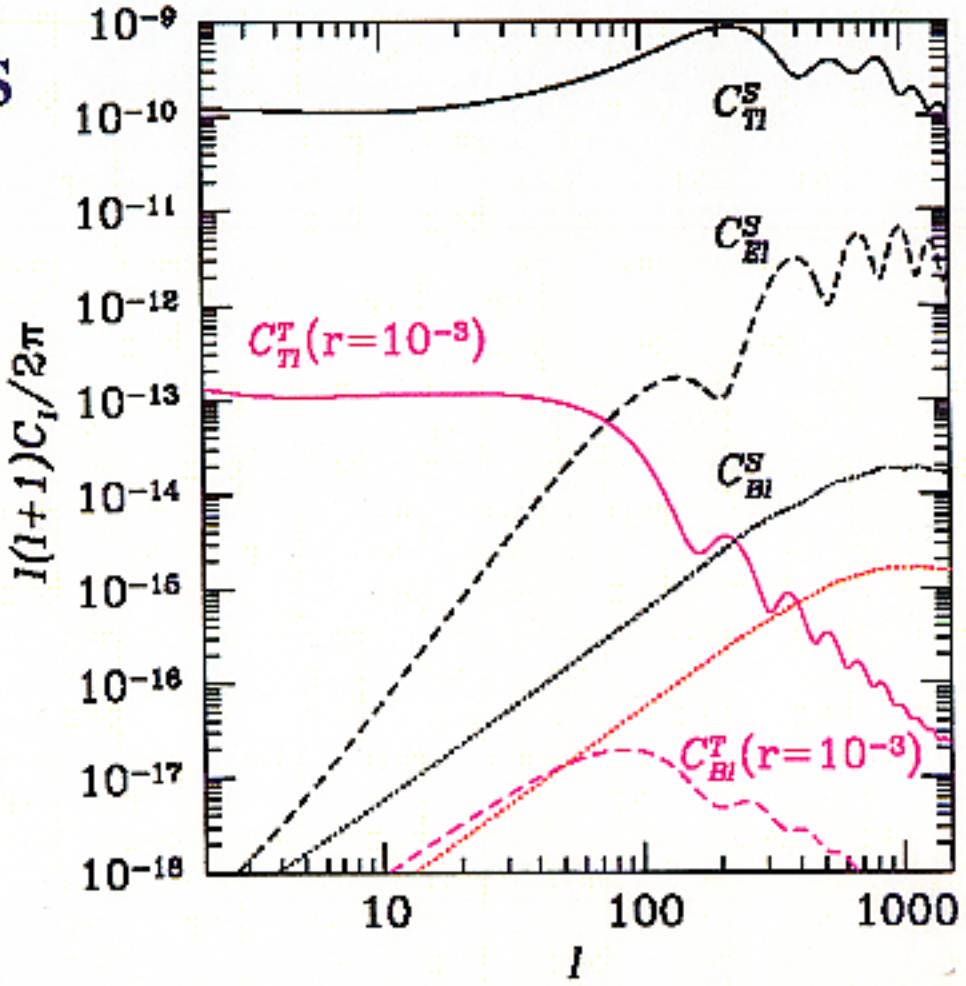

FIG. 1: Angular power spectra. Solid lines are for temperature anisotropies due to scalar perturbations, C_{Tl}^S and tensor perturbations, C_{Tl}^T with $r = 10^{-3}$. Dashed lines are for the E modes from scalar perturbations, C_{El}^S and the B modes from tensor perturbations, C_{Bl}^T. The dotted lines are for the lensing–induced scalar B-modes, C_{Bl}^S before (above) and after (below) the cleaning that can be done by a perfect experiment.

Knox & Song
astro-ph/0202286

Cleaning the B-Modes

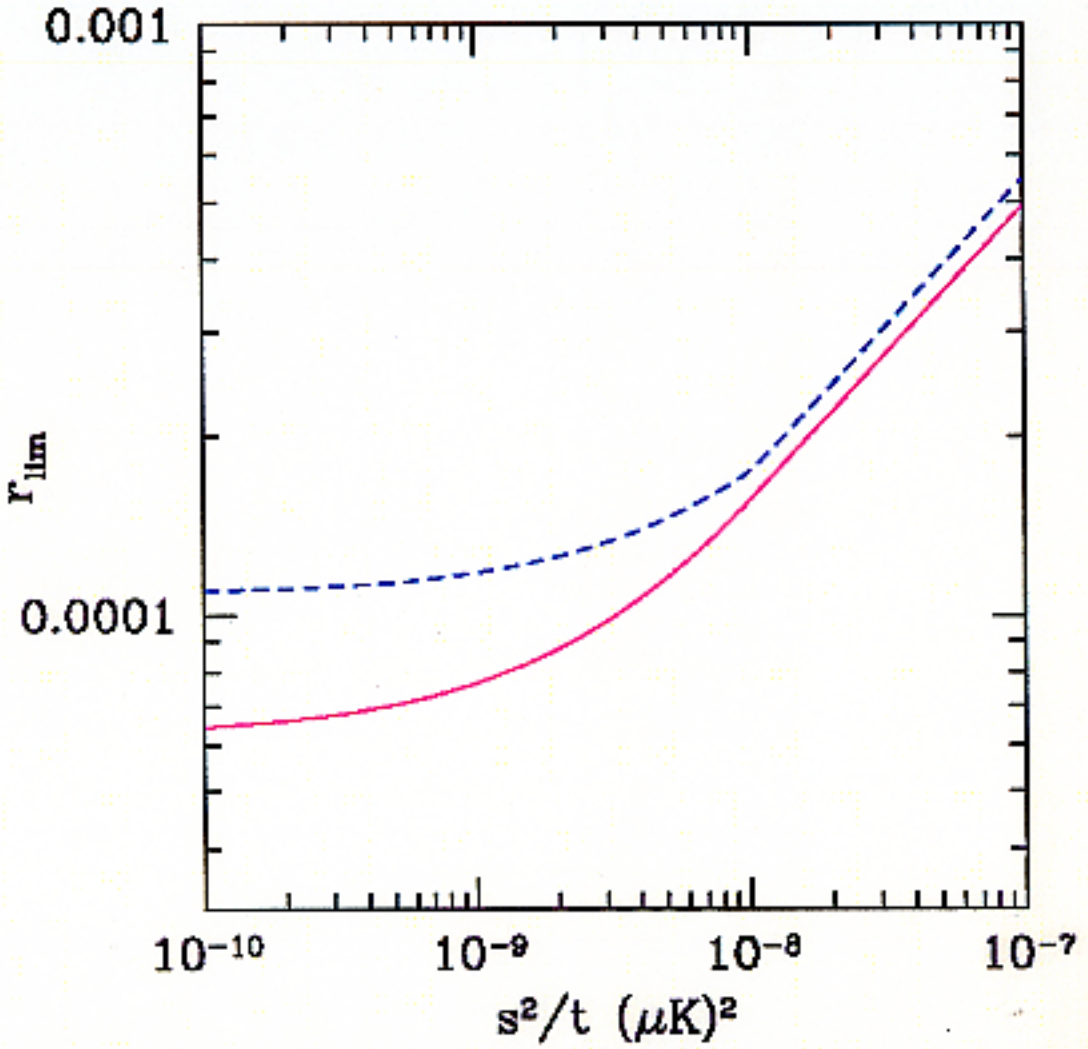

FIG. 3: Achievable detectability limit as a function of total detector array sensitivity, s and observing time t, assuming optimal sky coverage (lower curve) and 1/3 of optimal sky coverage (upper curve). Detectability limit assuming three times optimal sky coverage overlaps the upper curve when optimal sky coverage is less than 1/3.

Knox & Song
astro-ph/0202286